The BigBrain – an ultra-high resolution 3D human brain model

K. Amunts[1,2,3]*, Claude Lepage[4], Louis Borgeat[5], Hartmut Mohblerg[1], Timo Dickscheid[1], Marc-Étienne Rousseau[4], Sebastian Bludau[1], Pierre-Louis Bazin[6], Lindsay B. Lewis[4], Ana-Maria Oros-Peusquens[1], Nadim J. Shah[1], Thomas Lippert[7], Karl Zilles[1,2,3], Alan Evans[4]

Supporting Material:

Materials and Methods

1. Histological processing

We histologically processed a complete post-mortem human brain of a 65 year old female without any neurological or psychiatric diseases in clinical records (Fig. 1). The post-mortem brain was acquired through the body donor program of the University of Düsseldorf in accordance with legal requirements. It was removed during autopsy with a delay of 14 hours (fresh weight 1392 g) and was fixed in 4% buffered formalin for 5 months. MR imaging was performed prior to histological processing, in April 2003, to obtain an undistorted reference for further 3D-reconstruction of histological sections. The brain was placed in a custom-made Plexiglas cylinder with restraints designed to prevent motion during scanning and kept in formalin for best preservation of tissue. Extensive degassing of the formalin solution was performed prior to scanning in order to eliminate air bubbles which can adhere to the surface of the brain, induce susceptibility-related artifact in MR images and thus deteriorate the definition of the surface. A 1.5T scanner was used for MRI using a transmit body coil and a 12-channel receiver coil. The manufacturer's MPRAGE sequence was used with parameters including: TR=2220 ms, TE=3 ms, IR=1200 ms, flip=15 deg, resolution 0.4 x 0.4 x 0.8mm^3 and 6 averages. Whereas with considerable effort it was possible to produce images at a resolution of 0.3 mm^3 and with high contrast and SNR even at 1.5T (*1*), the MPRAGE images with moderately high resolution were found to be adequate for brain surface reconstruction.

In contrast to a recent mouse brain project, where imaging and sectioning were performed simultaneously without collecting sections (*2*), it is not feasible to process a complete human brain sections in such a manner. Here, the brain was embedded into paraffin and sectioned, from posterior to anterior, with a large-scale microtome in the coronal plane (thickness: 20 μm; total of 7,404 sections; occipital sections have low section numbers, frontal have high numbers). For optimal quality, sections were transported on a home-made conveyor system, and then transferred to wooden plates (Fig. 1D). To make the thin sections more visible, the whole brain was stained red with eosin. Subsequently, the eosin was removed from the mounted histological sections. Every section was collected, mounted, and stained for cell bodies (Fig. 1G-I) applying a silver staining method (*3*). The Merker staining is comparable to the classical Nissl staining, but gives a higher contrast between cell bodies and neuropil. The amount of lost sections was in the range of 0.5%. Each stained histological section was scanned on a flatbed scanner at 2,400 dpi in 16 bits, resulting in an in-plane resolution of 10 μm and a histological data set of ~800 Gb. It took 5-10 minutes for digitalization and storage per section, resulting in a total scanning time of approximately 1,000 hours. Downscaled 16-bit images with an in-plane resolution of 20 μm occupy 250 Gb.

Each blockface of the paraffin-embedded brain was digitized using a CCD-camera (objective "tarcus" 35 mm 1:2,8.), resulting in the same number of blockface images (image matrix: 512 x 480 pixels, resolution: ~0.5 mm/pixel, dynamic range: 8 bit). The images were stored in tiff-format (~1.4 Gb). The stacked blockface images served as an undistorted 3D reference to which the MRI volume was registered and virtually sectioned for subsequent shape reconstruction of the stained histological sections (see below, 3D-reconstruction).

2. Three-dimensional reconstruction of histological sections

The 3D reconstruction of the histological sections was two-fold: first, the artifacts were corrected in the original sections; second, the corrected sections were aligned using section-to-section registration (Fig. S2). A flowchart of the overall process is pictured in Fig. S3.

The images of the original histological sections were first repaired (at full 10 μm resolution) to remove sectioning artifacts. Sections with large displaced pieces were edited manually to align the major dislocated pieces prior to the application of an automatic repair procedure for correcting smaller defects. The manual editions were performed using in-house tools. The automatic repair algorithm, also developed in-house, relies on non-linear section-to-section registration of neighboring sections to detect and correct artifacts. The multi-scale registration is performed using *minctracc,* calibrated and optimized for 2D histological sections (http://en.wikibooks.org/wiki/MINC/Tools/mni_autoreg). For each section, its three immediate previous and post neighboring sections were registered and intensity-normalized to the middle section. These normalized registered sections were averaged and outlier voxels were detected based on the local variance of the averaged intensities. A crucial issue for the detection of outliers was not to consider the variance on a pixel-by-pixel basis (which is too sensitive to biological variations of the tissue and SNR), but to consider the total variance in a small neighborhood of n x n blocks (n=25 yields a block of 0.25mm x 0.25mm). Outliers were removed on a block-by-block basis by replacing the n x n block by the corrected average (median) of the neighboring sections, excluding outliers (outliers can be present in the reference section as well as in the neighboring sections). This process was repeated twice, using the repaired sections in the first iteration to improve the non-linear alignment and intensity normalization in the second iteration. Figure S2 shows a typical section at the various stages of the repair procedure. The final repaired section has been restored with high fidelity. This artifact correction procedure consumed 6 to 8 CPU hours per section.

The alignment of the repaired sections was accomplished in two steps. In the first step, the histological sections were registered to the corresponding sections of the MRI aligned to the blockface volume. This corrects for the vertical compression of the tissues in the slicing direction and aligns each section to its average position based on the MRI reference. In the second step, a multi-scale multi-resolution iterative algorithm is deployed to correct for the local displacement, distortion and stretch of sections relative to the MRI reference. In essence, the position and shape of a section are corrected to be at the mid-position of its immediate previous and next section neighbors. A minimum of 100 iterations were required to resolve all scales (Fig. S4). Calculations were performed on high performance (HPC) facilities within the Compute Canada network. The alignment of the entire brain (7,404 sections) required ~250,000 CPU hours.

Finally, intensity imbalances due to staining were corrected, to first-order, within each aligned section, then globally throughout the brain by histogram equilibration. Some residual intensity imbalances, however, persist in sections with poor gray-white matter contrast.

3. Definition of cortical borders in histological and image sections

Borders of cortical areas were defined using image analysis and statistical criteria (*4*). Borders have been defined in the sensorimotor, visual and auditory cortex as well as in higher

associative cortex (frontal lobe areas BA10/BA32). The borders were defined in the original sectioning plane and in the 3D-reconstructed horizontal or sagittal planes (Figs. 2 and 3). Profiles orthogonal to the surface were obtained, which captured the laminar changes in the optical density from the layerI/layer II border to the cortex/white matter border (Figs. 3E, F). Feature vectors were extracted from these profiles as measures of cytoarchitecture. Using a sliding window procedure, the Mahalanobis distance was measured between *n* neighboring groups of profiles (blocksize 11<=*n*<=24) in dependence on the position of the profile (Figs. 3G,H). The Mahalanobis distance was significant at the border between mesial BA10 and BA32 (Fig. 3I,J) as well as in primary sensorimotor, visual and auditory areas (Figs. 2D-G) independently of the blocksize.

The extraction of profiles running orthogonal to the cortical surface was performed on the basis of the optical density. We used the optical density as opposed to the GLI (grey level index (*5*)) applied in previous cytoarchitectonic studies (e.g. (*6*)), because the resolution of the BigBrain data set of 20 µm does not allow segmenting single cells from surrounding neuropil, a prerequisite for the measurement of the GLI (Fig. S1). To further investigate putative differences between density- and GLI-based measurements, the border between areas BA10/BA32 has been verified by the analyses of the original histological section with an in-plane resolution of 1 µm, and the GLI as a measure of the volume fraction of cell bodies (*7*). The corresponding coronal sections at 1µm were digitized using a light microscope with scanning stage. The GLI approach on the corresponding sections at 1µm showed identical positions of borders as in the BigBrain model with 20-µm isotropic volume using the optical density measurement, thus demonstrating that the quality of the 3D-reconstruction is good enough to detect changes in the laminar pattern at the border of two areas, although the fine morphology of single neurons is not visible at this spatial resolution (Fig. S1).

4. Visualization and data analysis

During the development of the 3D reconstruction pipeline, project collaborators located on different continents had to be able to frequently visualize different intermediate versions of the full size 3D brain model. The Atelier3D framework (https://cbrain.mcgill.ca/tools/atelier3d) was originally designed for collaborative visualization and analysis of large 3D datasets (*8, 9*) and was adapted to allow remote visualization of the BigBrain on desktop systems (Fig. S5). In Atelier3D, pre-processed spatial data is streamed on-demand from a remote server at sufficient resolution to render precise imagery on the client side, making scale issues transparent to the remote users. Furthermore, to facilitate data validation and analysis, specific visualization modes were implemented to mimic the interface of more classical volume and histology analysis software, providing options to combine axial or oblique cuts, direct volume renderings and processed data such as surfaces or profiles previously extracted from the volume (see movie S1).

The processing pipelines and tools run not only at the HPC facilities within the Compute Canada network (https://computecanada.ca/index.php/en/), but have also been readily implemented to run on JUROPA (http://www.fz-juelich.de/ias/jsc/EN/Home/home_node.html). JUROPA is a highly efficient cluster computer providing large centralized compute capacity in excess of 25,000 CPU-cores, as well as co-located parallel online storage in the Petabyte range. The advantage of this platform is that it allows for data-intensive computations as well as long-term storage of the results, thus avoiding extensive data movement in the subsequent analysis of

the data set, such as the extraction of stereological parameters, cortical surfaces, etc.

Public access is provided through the CBRAIN Portal (http://bigbrain.cbrain.mcgill.ca) upon free subscription. This enables the users with HTTP and SFTP to access the entire sets of stacked 2D data (coronal, axial and sagittal sections at 20 µm sampling and 16-bit dynamic range). The dataset will initially be available in Portable Network Graphics (png) or Medical Imaging NetCDF (MINC) formats, with the largest coronal sections occupying 35 MB each. Assembled 3D volumes at 100, 200, 300, 400 µm are available in MINC and NIfTI formats. We will provide direct cloud-based Web-Services access to the raw data, allowing connectivity from other platforms and databases.

5. Normalization to MNI space

The resampled 3D stack of BigBrain sections with 400 µm isotropic (recursive averaging over nine consecutive sections) was normalized to MNI space. The reconstructed volume exhibited a contrast between gray and white matter similar to that of quantitative T1 MRI. Accordingly, for stereotaxic normalization, we used a group-averaged T1 map obtained from 24 normal subjects who were scanned at 700 µm on a 7T scanner with the MP2RAGE sequence (*10*). Individual brain volumes were co-registered to MNI space at 400 µm to obtain a groupwise quantitative T1 average atlas. The BigBrain volume was then processed with N3 (*11*) to correct for remaining inhomogeneities in staining intensity after averaging. Non-brain regions close to brain tissue were labeled and assigned an arbitrary intensity value so as to be comparable with CSF regions in the stereotaxic T1 atlas. Finally, the processed BigBrain volume was co-registered to the T1 atlas at 400 µm with the SyN algorithm (*12*) using a cross-correlation image similarity criterion. The normalized BigBrain data are available at: (http://bigbrain.cbrain.mcgill.ca).

Fig. S1: Comparison of the level of detail in a cortical region of interest at 1 μm (A; microscopical resolution), 20 μm isotropic (B, resolution of the Big Brain dataset) and 500 μm (C, typical of high-resolution MRI of the human brain).

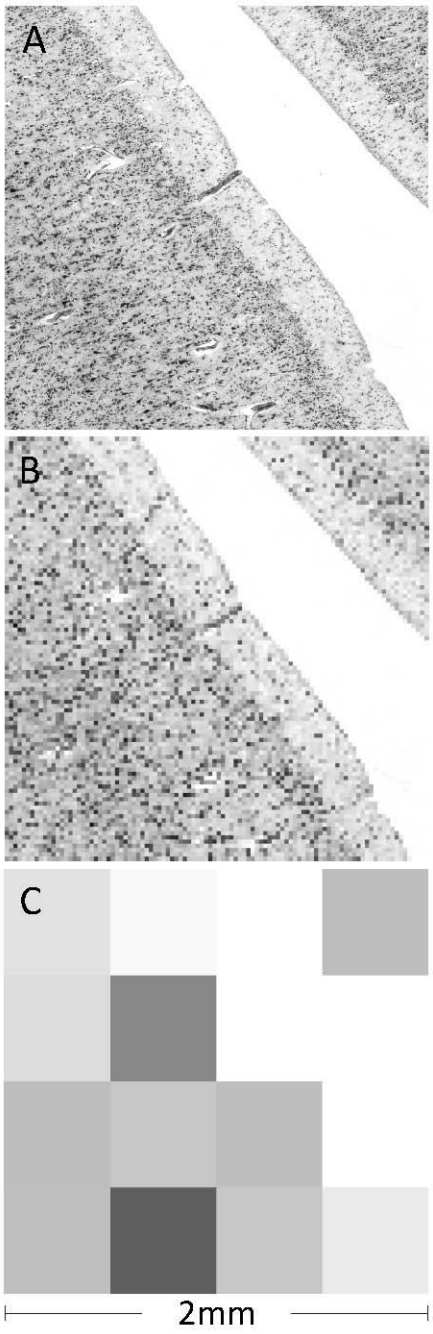

Fig. S2: Repair procedure in a histological section. (A) Original image, showing several artifacts including a deep rupture with displacement and distortion of the tissue as well as inhomogeneity in staining intensity. (B) The most prominent artifacts were removed by manual repair. (C) An automated repair procedure and an intensity correction allowed reconstruction of the image with high quality (see also Fig. S3).

Fig. S2

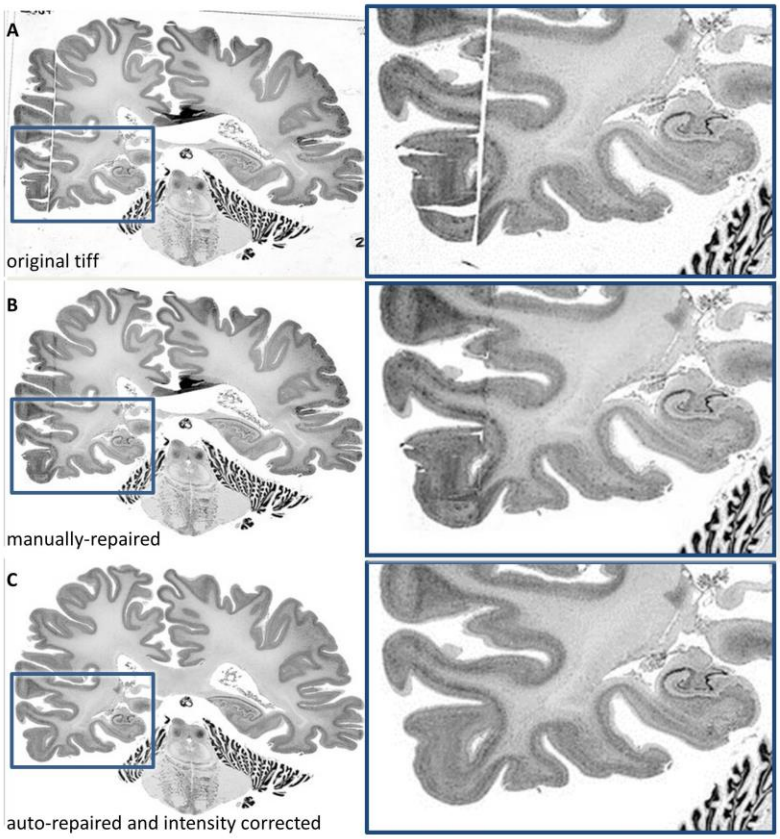

Fig. S3: Flowchart of the image processing pipeline. QC – decision; if QC=yes, go to the next step; if QC=no, repeat the process. Square boxes are global processes, like the main steps. The boxes with rounded corners are sub-processes of the main one. Dashed lines indicate a "weak" connection; for example, the 3-D alignment to MRI is "weakly" used in the masking stage.

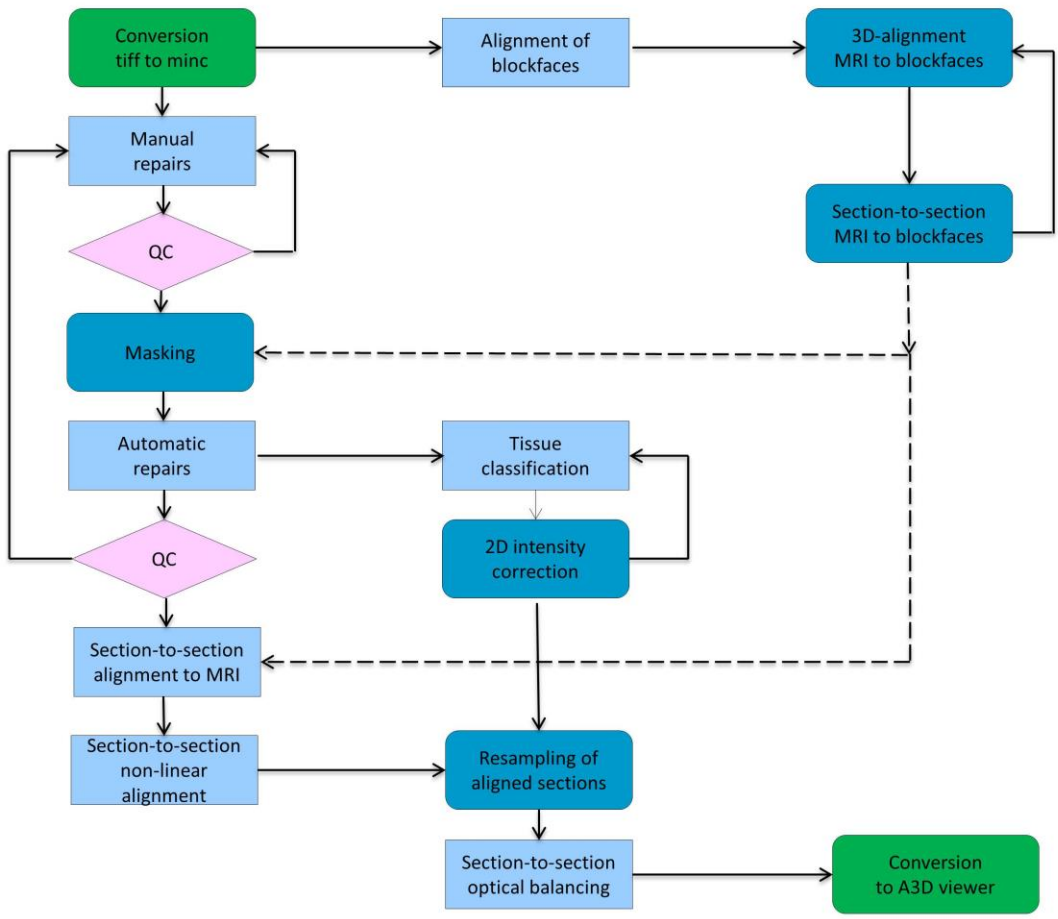

Fig. S4: Convergence residual of 3D-reconstruction with respect to the section number. The residual is the change in cross-sectional area of consecutive aligned sections. Section areas grow, and then decay in size from one end to the other (posterior-anterior). The ideal curve would be smooth with no oscillations, showing how the brain grows in cross-sectional area from posterior to anterior. The levels of alignment go from initial alignment to MRI (red curve) then to successively finer grids (coarse, medium, fine corresponding to levels of 200, 100, and 50 μm, respectively (green, blue and purple curves). Important is the trend of the graph, showing a better alignment from step to step.

Fig. S4

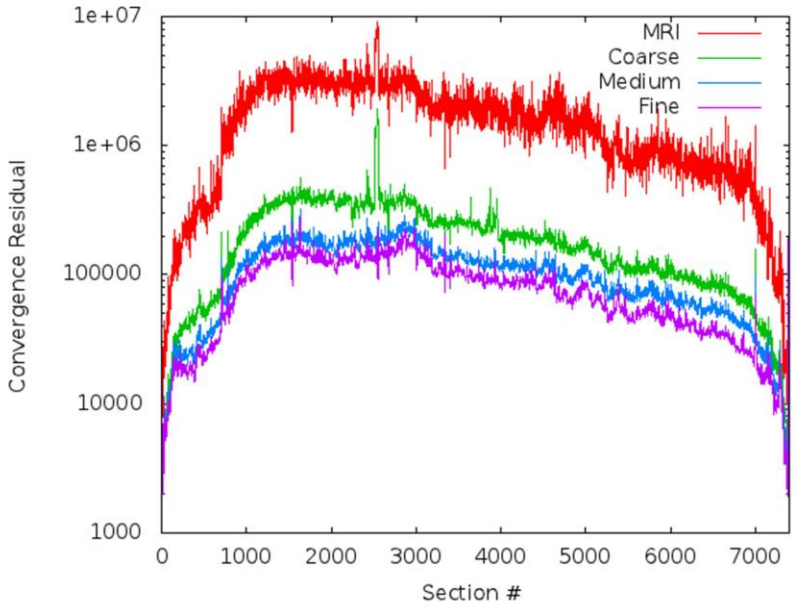

Fig. S5: Screenshot from Atelier3D (*9*) with virtual sagittal and horizontal sections reconstructed from the originally acquired coronal series of 7404 sections. Note the smooth contours in the virtual sections indicating the high quality of 3D-reconstruction. Lower right: surface reconstruction of the digital whole human brain with 0.02 mm isotropic resolution, whereby the sectioning planes are labeled by red lines on the brain surface.

Figure S5

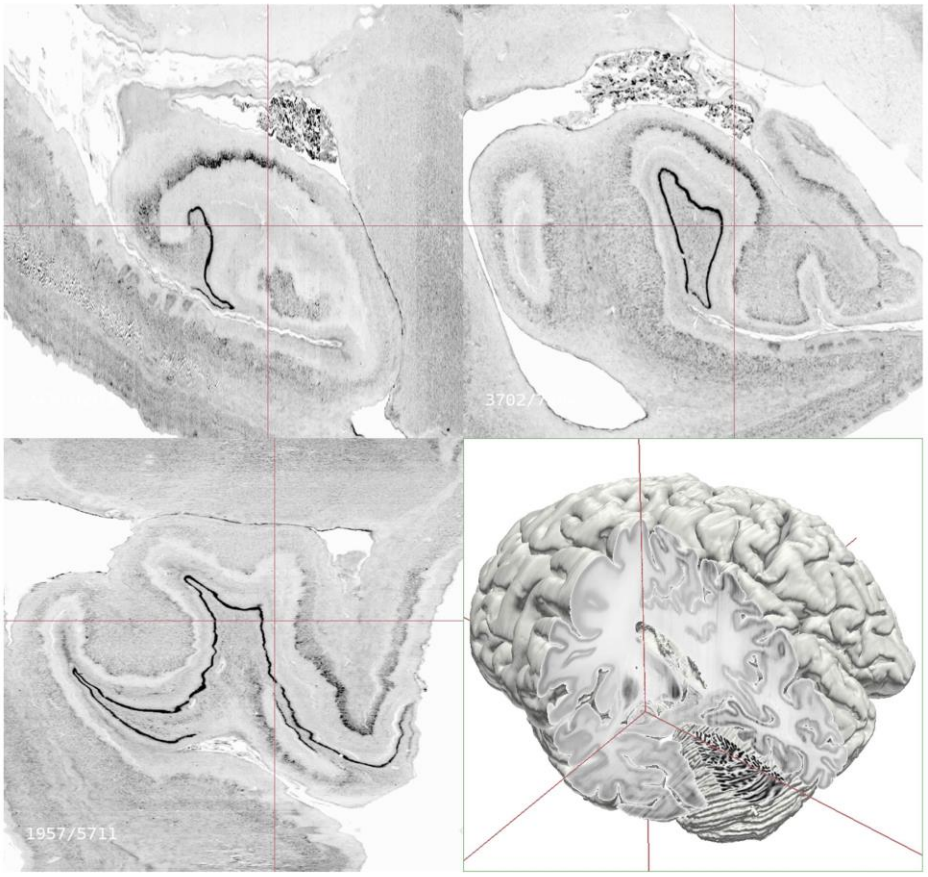

Fig. S6: Co-registration of the BigBrain in stereotaxic space, shown in 3 cardinal axes.
Top: Superposition of BigBrain and stereotaxic quantitative T1 group-average map. Middle: BigBrain; Bottom: Stereotaxic quantitative T1 group-average map.

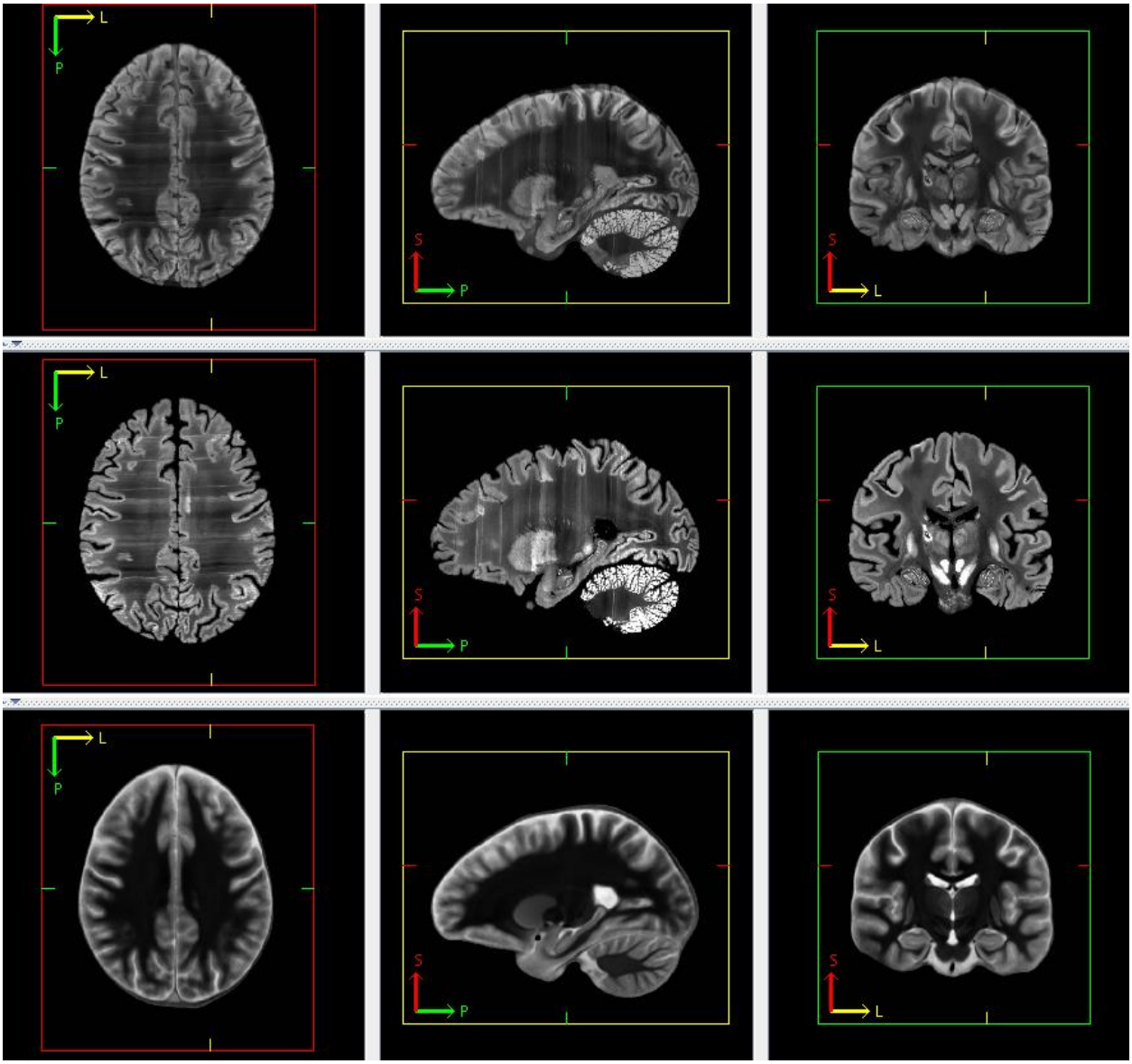

Movie S1: Visualization of the 3D-reconstructed data set of the BigBrain from Atelier3D.

Reference List

1. A. M. Oros-Peusquens, T. Stoecker, K. Amunts, K. Zilles, N. J. Shah, *Magn. Res. Im.* **28**, 329 (2010).
2. D. Mayerich, L. Abbot, B. McCormick, *J. Microsc.* **231**, 134 (2008).
3. B. Merker, *J. Neurosci. Meth.* **9**, 235 (1983).
4. A. Schleicher, P. Morosan, K. Amunts, K. Zilles, *J. Autism. Develop. Disord.* **39**, 1568 (2009).
5. A. Wree, A. Schleicher, K. Zilles, *J. Neurosci. Meth.* **6**, 29 (1982).
6. P. Morosan *et al.*, *Neuroimage* **13**, 684 (2001).
7. A. Schleicher *et al.*, *Anat. Embryol.* **210**, 373 (2005).
8. L. Borgeat *et al.*, *IEEE Comput. Graph. Appl.* **27**, 60 (2007).
9. L. Borgeat *et al.*, ETH Zürich, 2007).
10. J. P. Marques *et al.*, *Neuroimage* **49**, 1271 (2010).
11. J. G. Sled, A. P. Zijdenbos, A. C. Evans, *IEEE Trans. Med. Imaging* **17**, 87 (1998).
12. B. B. Avants, C. L. Epstein, M. Grossman, J. C. Gee, *Med. Image Anal.* **12**, 26 (2008).